Accepted for publication. DOI: 10.1109/IEEE-IWS.2018.8400878

Constant Capacitive Wireless Power Transfer at Variable Coupling

Ben Minnaert*, Franco Mastri†, Mauro Mongiardo‡, Alessandra Costanzo†, and Nobby Stevens*,
*KU Leuven, DRAMCO, Dept. of Electrical Engineering, 9000 Ghent, Belgium
E-mail: ben.minnaert@kuleuven.be; nobby.stevens@kuleuven.be
†Dept. of Electrical, Electronic and Information Engineering
Guglielmo Marconi, University of Bologna, 40136 Bologna, Italy
E-mail: franco.mastri@unibo.it; alessandra.costanzo@unibo.it
‡Dept. of Engineering, University of Perugia, 06123 Perugia, Italy
E-mail: mauro.mongiardo@unipg.it

***Abstract*—Capacitive wireless power transfer uses the varying electric field for wireless power transfer from a transmitter plate to a receiver plate. The amount of power transferred to the load and the system efficiency are dependent of the coupling between transmitter and receiver. However, by changing the operating frequency, it is possible to achieve constant power transfer and efficiency, even at variable coupling. In this work, the analytical expressions for the three different gains of a general capacitive wireless power transfer system are calculated. Based on the gains, an analytical solution is determined for achieving constant power transfer and efficiency at variable coupling. The analytical results are validated by circuital simulation in SPICE.**

***Index Terms*—capacitive wireless power transfer, coupling factor, resonance, power transfer, wireless power transfer.**

I. Introduction

Wireless power transfer (WPT) has several advantages compared to wired charging [1]–[3]:

- WPT results in an improved convenience and user experience, especially for portable electronics.
- Wireless charged devices can achieve a higher durability and robustness since no open connections are necessary. The device can be sealed entirely, making it water and dust proof.
- Wired charging can generate sparks when (dis)connecting the charging cable to the device. WPT can increase safety in hazardous industrial environments where flammable or combustible atmospheres are present, for example at chemical plants.
- WPT can facilitate the miniaturization of devices due to the omission of a large charger connector or a reduction in battery size.
- For certain applications (e.g., medical implants, sensor networks), it can be costly, hazardous or infeasible to replace the batteries of the device or to connect charging cables.
- Smart devices are able to detect their low battery supply and can automatically report to a charging station to reload (e.g., automated guided vehicles, robots, drones,...). WPT allows the charging of these smart devices without any human involvement, leading to more flexible, reliable and energy-efficient operations.

WPT also has some drawbacks:

- Charging points for wired power transfer (electrical outlets) are abundant and standardized within each country. Wireless charging points are more scarce.
- Even though high efficiencies are realized with WPT, the efficiency is lower than wired charging.
- Since extra transmitters and receivers are necessary, the implementation cost of WPT is generally higher than wired charging.
- In general, wireless power transfer will produce more heat, which can lead to higher requirements for the material selection and/or a faster device degradation.

Two near-field WPT techniques exist:

- By means of a varying magnetic field, inductive wireless power transfer (IPT) realizes energy transfer from a transmitter coil to a receiver coil. IPT applications have already entered the market.
- Capacitive wireless power transfer (CPT) uses the electric field for the power transfer from a transmitter plate to a receiver plate. Compared to IPT, CPT technology allows for WPT through metal and could possibly be implemented at a lower cost than IPT [4], [5].

In this work, the analytical expressions for the three different gains of a general CPT system are calculated. The analytical solution is determined for achieving constant power transfer with the CPT technique: as well the system efficiency as the amount of power transfer remain constant, even for variable coupling between transmitter and receiver. For IPT, this has already been studied in detail [6], [7], but for CPT, a rigorous solution is lacking.

II. Methodology

A basic CPT system is represented by the circuit of Fig. 1. WPT is realized by the coupled capacitances C_1 and C_2. The coupling factor k is given by:

$$k = \frac{C_M}{\sqrt{C_1 C_2}} \tag{1}$$

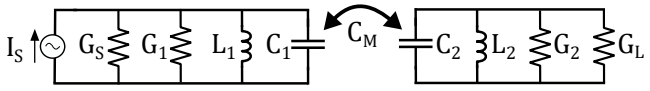

Fig. 1. Equivalent circuit representation of a basic CPT system.

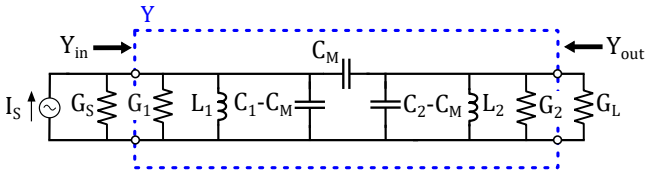

Fig. 2. Equivalent circuit of a basic CPT system, indicating the input admittance Y_{in} and output admittance Y_{out} .

with C_M the mutual capacitance. The measurement procedure to determine the value of these capacitances for a general CPT set-up can be found in [8].

I_S is a sinusoidal current source with angular frequency ω_0 and shunt conductance G_S. The losses in the transmitter and receiver are represented by the conductances G_1 and G_2, respectively. G_L is the load of the system. The value of the inductances L_1 and L_2 is given by (i=1,2):

$$L_i = \frac{1}{\omega_0^2 C_i} \tag{2}$$

It is important to note that the equivalent circuit of Fig. 1 is an approximation. A more accurate representation of inductor losses would require the introduction of series resistances. However, our approximation allows for a simple, analytical model with the goal of providing a first estimation of the system behavior.

Fig. 2 shows the equivalent circuit of Fig. 1. The indicated rectangle is considered as a two-port network with input admittance $Y_{in} = G_{in} + jB_{in}$, output admittance $Y_{out} = G_{out} + jB_{out}$, and admittance matrix $\mathbf{Y}$:

$$\boldsymbol{Y} = \begin{bmatrix} G_1 + \frac{1}{j\omega L_1} + j\omega C_1 & -j\omega C_M \\ -j\omega C_M & G_2 + \frac{1}{j\omega L_2} + j\omega C_2 \end{bmatrix} \tag{3}$$

Normalizations are performed according to Table I. The normalized frequency u is defined as:

$$u = \frac{\omega}{\omega_0} \tag{4}$$

A WPT network can be characterized by three gains [9]:

- The power gain G_P is given by the ratio between the power dissipated by the load and the input power. It corresponds to the efficiency of the WPT system.

TABLE I
NORMALIZED PARAMETERS

$g_1 = G_1/(\omega_0 C_1)$	$g_2 = G_2/(\omega_0 C_2)$
$g_S = G_S/(\omega_0 C_1)$	$g_L = G_L/(\omega_0 C_2)$
$g_{Tx} = g_1 + g_S$	$g_{Rx} = g_2 + g_L$
$g_{in} = G_{in}/(\omega_0 C_1)$	$g_{out} = G_{out}/(\omega_0 C_2)$
$b_{in} = B_{in}/(\omega_0 C_1)$	$b_{out} = B_{out}/(\omega_0 C_2)$

- The available gain G_A is defined as the ratio between the maximum available power at the output port of the network and the maximum available power of the generator.
- The transducer gain G_T is defined as the ratio between the power dissipated by the load and the maximum available power of the generator. It is therefore a measure for the power transfer to the load.

Following the same methodology as [6], the following expressions can be derived:

$$G_P = \frac{k^2 g_L u^4}{(g_1 + k^2 g_{Rx})u^4 + g_1(g_{Rx}^2 - 2)u^2 + g_1} \tag{5}$$

$$G_A = \frac{k^2 g_S u^4}{(g_2 + k^2 g_{Tx})u^4 + g_2(g_{Tx}^2 - 2)u^2 + g_2} \tag{6}$$

$$G_T = \frac{4k^2 g_S g_L u^6}{D} \tag{7}$$

with

$$D = [(1-k^2)u^4 - (2 + g_{Tx}g_{Rx})u^2 + 1]^2 + [(g_{Tx} + g_{Rx})u(1-u^2)]^2 \tag{8}$$

At the main resonant frequency ($u = 1$), the gains are given by:

$$G_P(u=1) = \frac{k^2 g_L}{g_{Rx}(k^2 + g_1 g_{Rx})} \tag{9}$$

$$G_A(u=1) = \frac{k^2 g_S}{g_{Tx}(k^2 + g_2 g_{Tx})} \tag{10}$$

$$G_T(u=1) = \frac{4k^2 g_S g_L}{(k^2 + g_{Tx}g_{Rx})^2} \tag{11}$$

The real and imaginary part of the normalized input admittance are:

$$g_{in} = g_1 + \frac{k^2 g_{Rx} u^4}{u^4 + (g_{Rx}^2 - 2)u^2 + 1} \tag{12}$$

$$b_{in} = \frac{(u^2-1)[(1-k^2)u^4 + (g_{Rx}^2 - 2)u^2 + 1]}{u[u^4 + (g_{Rx}^2 - 2)u^2 + 1]} \tag{13}$$

It can be seen that the input admittance is purely resistive if u equals unity. The corresponding angular frequency, ω_0, is called the main resonant frequency. However, b_{in} also becomes zero for the frequencies u that meet

$$(1-k^2)u^4 + (g_{Rx}^2 - 2)u^2 + 1 = 0 \tag{14}$$

This equation has solutions only if

$$g_{Rx} \leq \sqrt{2} \tag{15}$$

and

$$k \geq k_b = g_{Rx}\sqrt{1 - \frac{g_{Rx}^2}{4}} \tag{16}$$

TABLE II
SIMULATION PARAMETERS

$f_0 = 10$ MHz	$I_S = 1$ A
$C_1 = C_2 = 300$ pF	$L_1 = L_2 = 84.4\mu$H
$G_1 = G_2 = G_S = 188$ μS	$G_L = 2.83$ mS
$g_1 = g_2 = g_S = 0.01$	$g_L = 0.15$

Solving equation (14) results in

$$u_{\pm} = \sqrt{\frac{2 - g_{Rx}^2 \pm \sqrt{4k^2 + g_{Rx}^4 - 4g_{Rx}^2}}{2(1-k^2)}} \tag{17}$$

k_b and $u_{\pm}$ are called the bifurcation coupling and the secondary resonant frequencies, respectively.

At $u_{\pm}$, the normalized input admittance is real and equals

$$g_{in}(u = u_{\pm}) = g_1 + g_{Rx} \tag{18}$$

which is independent of the coupling factor k.

The power gain G_p and transducer gain G_T at the secondary resonant frequencies u=$u_{\pm}$ are given by:

$$G_P(u = u_{\pm}) = \frac{g_L}{g_1 + g_{Rx}} \tag{19}$$

$$G_T(u = u_{\pm}) = \frac{4g_S g_L}{(g_{Tx} + g_{Rx})^2} \tag{20}$$

Both G_P and G_T are independent of the coupling k at the secondary resonance frequencies. This was to be expected. The secondary resonance frequencies are chosen such that the input admittance is purely real, i.e. b_{in}=0. Under those circumstances, the network behaves purely resistive and is therefore independent of the coupling (i.e., independent of the mutual capacitance C_M).

On the contrary, the available gain G_A at $u_{\pm}$ is dependent of the coupling k. Indeed, G_A is defined as function of the maximum available power at the output port. Since this power is dependent of the output admittance, and $B_{out} \neq 0$, the coupling factor k will influence its value.

III. CIRCUITAL VALIDATION

Fig. 3 plots G_P and G_T as function of the coupling factor k for a system with the values of Table II. The continuous lines show the values at the main resonant frequency $u = 1$. The horizontal dashed lines show G_P and G_T at the secondary resonant frequencies $u_{\pm}$. Both G_P and G_T remain constant at 88.2% and 18.5%, respectively. In other words, the efficiency and power transfer remain constant for variable coupling, as long as $k \geq k_b$. A higher power transfer to the load is possible, compared to the configuration operating at the main resonant frequency. As a consequence, a decrease in efficiency is observed, but the difference with the efficiency at main resonant frequency is limited.

The analytical derivation is verified by circuit simulation in SPICE. First, the circuit simulation at the main resonant frequency f_0 of 10 MHz is performed. The crosses in Fig. 3

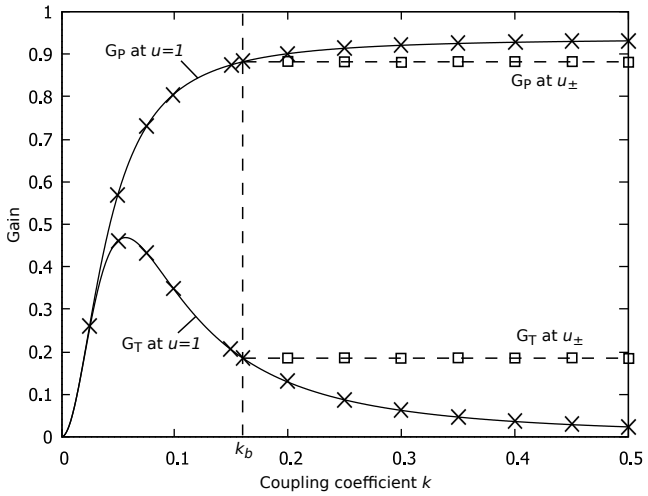

Fig. 3. The continuous lines show the gains G_P and G_T (equations (9) and (11)) at the main resonant frequency u=1 as function of the coupling coefficient k for the example configuration. The dashed lines indicate the values at the secondary resonant frequencies $u_{\pm}$, valid for $k \geq k_b$ (equations (19) and (20)). The crosses and squares show the circuit simulation results for the main and secondary frequencies, respectively.

show the simulation results. A perfect agreement is found with the analytical derivation.

Secondly, the two secondary frequencies $u_{\pm}$ are determined for each k. For example, at k =30%, the secondary frequencies are 8.98 MHz and 11.7 MHz. For varying coupling factors, the SPICE simulation is performed for both their secondary frequencies. The results are plotted in Fig. 3 as squares. Again, a perfect agreement with the analytical derivation is found.

IV. CONCLUSION

The analytical expressions for the three different gains of a general CPT system were calculated. Based on the gains, the solution for achieving constant power transfer at variable coupling is determined. It provides a simple model, allowing a first estimate for a constant power transfer design. Compared to the main resonant frequency mode, operating the system at the secondary frequencies allows for a constant power transfer at variable coupling at the expense of a small efficiency decrease.

REFERENCES

[1] X. Lu, P. Wang, D. Niyato, D. I. Kim, and Z. Han, "Wireless charging technologies: Fundamentals, standards, and network applications," *IEEE Communications Surveys & Tutorials*, vol. 18, no. 2, pp. 1413–1452, 2016.

[2] A. M. Jawad, R. Nordin, S. K. Gharghan, H. M. Jawad, and M. Ismail, "Opportunities and challenges for near-field wireless power transfer: A review," *Energies*, vol. 10, no. 7, p. 1022, 2017.

[3] S. D. Barman, A. W. Reza, N. Kumar, M. E. Karim, and A. B. Munir, "Wireless powering by magnetic resonant coupling: Recent trends in wireless power transfer system and its applications," *Renew. Sust. Energ. Rev.*, vol. 51, pp. 1525–1552, 2015.

[4] B. Minnaert and N. Stevens, "Conjugate image theory applied on capacitive wireless power transfer," *Energies*, vol. 10, no. 1, p. 46, 2017.

[5] C. Liu, A. Hu, and N.-K. Nair, "Modelling and analysis of a capacitively coupled contactless power transfer system," *IET power electronics*, vol. 4, no. 7, pp. 808–815, 2011.

[6] F. Mastri, A. Costanzo, and M. Mongiardo, "Coupling-independent wireless power transfer," *IEEE Microw. Compon. Lett.*, vol. 26, no. 3, pp. 222–224, 2016.

[7] W. Zhang, S.-C. Wong, K. T. Chi, and Q. Chen, "Analysis and comparison of secondary series-and parallel-compensated inductive power transfer systems operating for optimal efficiency and load-independent voltage-transfer ratio," *IEEE Trans. Power Electron*, vol. 29, no. 6, pp. 2979–2990, 2014.

[8] L. Huang and A. P. Hu, "Defining the mutual coupling of capacitive power transfer for wireless power transfer," *Electronics Letters*, vol. 51, no. 22, pp. 1806–1807, 2015.

[9] F. Mastri, M. Mongiardo, G. Monti, and L. Tarricone, "Characterization of wireless power transfer links by network invariants," in *Electromagnetics in Advanced Applications (ICEAA), 2017 International Conference on*. IEEE, 2017, pp. 590–593.